Nuclear Inst. and Methods in Physics Research, A 875 (2017) 80–86

Contents lists available at ScienceDirect

Nuclear Inst. and Methods in Physics Research, A

journal homepage: www.elsevier.com/locate/nima

Quasi-monoenergetic ultrashort microbunch electron source

Levi Schächter [a,*], Wayne D. Kimura [b]

[a] Department of Electrical Engineering, Technion – Israel Institute of Technology, Haifa 32000, Israel
[b] STI Optronics, Inc., 2647 151st Place NE, Redmond, WA 98052, USA

ARTICLE INFO

Keywords:
Electron sources

ABSTRACT

By combining static electric and laser fields for generation of field-emitted electrons, it is possible to generate a quasi-monoenergetic train of electron microbunches by controlling the anode–cathode spacing such that the time of flight of the electrons becomes independent of the laser field. Such quasi-monoenergetic microbunches with pulse durations that are a fraction of the laser wavelength would be ideal for radiation sources as well as compact accelerators.

1. Introduction

A train of electron bunches plays a pivotal role in many novel radiation sources as well as in advanced acceleration paradigms [1–4]. Ideally, the microbunch length should be a small fraction of the driving laser wavelength and it should have a narrow energy spread (i.e., quasi-monoenergetic) in order to be accelerated uniformly or produce a narrow radiation spectrum (quasi-monochromatic) [5–8].

A prime example where a train of fs-microbunches separated by the laser wavelength is needed is as an electron injection source for dielectric laser accelerators (DLA) [4]. The electric field within the channels of the DLA accelerating structure oscillates at the laser frequency. Hence, only electrons at the proper phase with respect to this field are accelerated and this optimum phase point has a periodicity equal to the laser wavelength. Moreover, the channel gap size is only of order one wavelength; hence, the emitter area of the injection source should also be this same order of size to maximize injection of the electrons into the channel.

One way to produce fs-microbunches is by combining static field emission with the oscillating electric field of a laser beam. The latter propagates parallel to the diode's electrodes and with the electric field perpendicular to both the cathode and the anode. Each one of the two electric field components, on its own, is not sufficient to generate significant field emission from the cathode. In fact, when the oscillating field is anti-aligned with the static field, emission is suppressed. Thus, significant electron emission only occurs during a fraction of each half-cycle of the laser field, thereby generating a train of ultrashort fs-microbunches separated in time by the period of the laser.

This basic scheme of combining a static field and oscillating field from a laser beam on a cathode has been experimentally demonstrated by several different research teams [9–11] and is essentially an extension to optical wavelengths of earlier work done using microwaves [12–14]. Hommelhoff, et al., [9] demonstrated several key attributes of this process: (i) Emission of electrons during a half-cycle of the laser field from tungsten cathodes, (ii) generation of electron pulses of 1 fs duration, and (iii) an average of about 200 electrons per microbunch corresponding to 3×10^{15} electrons per second for the mode-locked 1-GHz laser that was being used. It was also pointed out that their results yielded current densities and invariant brightnesses comparable to photocathodes, which implies that space-charge effects are manageable.

Ganter, et al., [10], demonstrated high peak currents (2.9 A) and indicated that low normalized emittances (< 0.05 mm-mrad) are feasible. These approaches were also quite different from that of Hernandez-Garcia and Brau [15–17] who demonstrated photoelectric field emission from needle cathodes where the laser intensity dominated over the field emission and could even damage the cathode.

This work by others on laser-driven field emitters with arbitrary choice of parameters did not result in an electron beam (*e*-beam) source suitable for injecting into an acceleration structure. One key characteristic they lacked was generating microbunches with low energy spread. We demonstrate in this quasi-analytic study that a proper choice of the static and oscillating electric field components results in an improved microbunches generation scheme. The three main characteristics of this paradigm are: (i) quasi-monoenergetic electrons can be emitted from the laser-driven field emitters by controlling the anode–cathode (A–K) gap size, and the static and oscillating field as well as the space-charge in

* Corresponding author.
E-mail addresses: levi@ee.technion.ac.il (L. Schächter), wkimura@stioptronics.com (W.D. Kimura).

http://dx.doi.org/10.1016/j.nima.2017.08.041
Received 8 June 2017; Received in revised form 16 August 2017; Accepted 22 August 2017
Available online 8 September 2017
0168-9002/

the diode. (ii) Accounting for the global (static) space-charge effect, we demonstrate within an excellent approximation that the bunch profile can be considered Gaussian. (iii) The transverse dynamics of the bunch is established and the normalized emittance is shown to be conserved along the diode gap.

2. Simplified 1D model – "resonant particle"

Our fundamental assumption is that the electron emission is governed by field emission rather than photo-emission thus throughout this study we rely on the Fowler–Nordheim (FN) equation [18] as adapted by Barbour, et al., [19] for tungsten,

$$J^{(\mathrm{FN})} = J_0^{(\mathrm{FN})}\left[\frac{F}{F_{\mathrm{cr}}(F)}\right]^2 \exp\left[-\frac{F_{\mathrm{cr}}(F)}{F}\right] \tag{1}$$

where F (V/cm) is the effective electric field that acts locally on the surface of the cathode, $J_0^{(\mathrm{FN})}\mathrm{A/cm}^2 = 7.18\times10^9\phi^2 f^2(y)$, ϕ is the work function (eV), which for tungsten has a value of 4.5 eV, $F_{\mathrm{cr}}(F) = 6.83\times10^7\phi^{3/2}f(y)$, and $f(y)$ is an elliptic function of the variable $y = 3.79\times10^{-4}F^{1/2}\phi^{-1}$; this function accounts for the effects of the mirror-image potential [20–22].

Although the FN equation was developed for static conditions, it is still valid for short pulses because the tunneling time it takes the bound electron to traverse the potential barrier is much shorter than one period of the laser field. Furthermore, the effective electric field F includes the field enhancement factor (β) that increases the magnitude of the applied field E, i.e., $F = \beta E$ and it accounts for the roughness and other geometric effects on the emitting surface.

In the framework of the 1D model, we consider a one-dimensional (1-D) geometry (see Fig. 1) that utilizes a cathode consisting of carbon nano-tubes (CNTs) spread over the cathode surface. These CNTs have demonstrated [23,24] enhancement factors much larger than the ones assumed here. Moreover, the CNTs can be deposited over a cathode area small on the scale of the wavelength (λ_0) of the illuminating laser e.g., $0.5\lambda_0\times0.5\lambda_0$ [25]. Such a cathode will produce an electron beam well matched to the small entrance opening of a realistic dielectric laser accelerator [4] structure $\sim\lambda_0$.

For our 1-D analysis, however, we assume with reference to Fig. 1 that the vertical size of the cathode region filled with CNTs is much less than the laser wavelength whereas the horizontal size is much longer than one laser wavelength. The anode–cathode (A-K) gap might be many laser wavelengths long e.g., $g\sim1$ mm, and the laser beam fills the entire A-K gap with its electric field oriented perpendicular to the cathode surface. As explained subsequently, if we assume a laser wavelength of $\lambda_0\sim10\,\mu$m and a laser pulse duration of $\tau_{L,p}\sim30$ ps then, as illustrated schematically in Fig. 1, there will be a train of hundreds of microbunches traveling within the A-K gap during the laser pulse. This is in contrast to the work by Hommelhoff, et al., [9], [26] where femtosecond laser pulses were used, thereby limiting the number of microbunches traveling within the A-K gap to only a few. This train of microbunches will affect the electron emission and microbunch characteristics through charge shielding and space charge spreading. These effects will be included in our analysis below.

In order to convey the essence of our concept we ignore momentarily the charge shielding and transverse effects. The field between the cathode and anode consists of the superposition of the static field, $E_{\mathrm{st}} = V_{\mathrm{st}}/g$, and the laser field, E_{L}, so that the net field $E(t)$ is given by

$$E(t) = -E_{\mathrm{st}} - E_{\mathrm{L}}\cos(\omega t+\psi) \tag{2}$$

where $\omega = 2\pi c/\lambda_0$ is the laser frequency and t is time; g is the A-K spacing. It is important to point out here that full control of the phase (ψ) is assumed. In other words, $t = 0$ represents the instant the net effective field on the cathode is the largest. Furthermore, the motion of the electrons in the direction parallel to the propagation of the wave (x) is ignored. Without loss of generality, we conceive that the emitting strip represented by our 1D cathode is located at the maximum of the

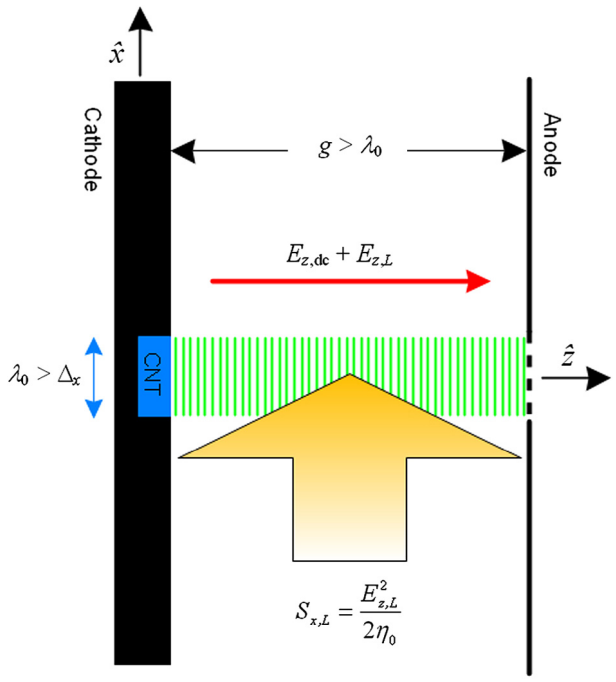

Fig. 1. (Color online) Schematic of the conceived optical injector: On the left the cathode consists of a polished metal with a narrow strip of carbon nano-tubes (CNT). This strip alone emits electrons every half cycle of the laser field; edge effects are neglected in the framework of this model. The A-K gap is designed such that each microbunch traverses the gap in an integer number of laser periods. Consequently, the kinetic energy of the emerging electrons is independent of the laser amplitude. (For interpretation of the references to color in this figure legend, the reader is referred to the web version of this article.)

propagating electric field namely, $E_{\mathrm{L}}\cos(\omega t) = \left\{E_{\mathrm{L}}\cos\left[\omega(t-x/c)\right]\right\}_{x=0}$ or for the case of a *standing* wave $E_{\mathrm{L}}\cos(\omega t) = E_{\mathrm{L}}\left[\cos(\omega t)\cos(\omega x/c)\right]_{x=0}$. Subject to the assumption mentioned above, in the cathode–anode gap, the equation of motion of the ith electron emitted at $t = 0$ is

$$\frac{d^2z_i}{dt^2} = \frac{e}{m}\left[E_{\mathrm{st}} + E_{\mathrm{L}}\cos(\omega t+\psi_i)\right] \tag{3}$$

whose solution, subject to the initial conditions $z_i(t=0) = 0$ and $\dot{z}_i(t=0) = 0$, is straightforward

$$z_i(t) = \frac{e}{m}\left\{E_{\mathrm{st}}\frac{1}{2}t^2 - \frac{E_{\mathrm{L}}}{\omega^2}\left[\cos(\omega t+\psi_i) - \cos(\psi_i) + \omega t\sin(\psi_i)\right]\right\}. \tag{4}$$

Provided the electrons are not impinging back on the cathode, the time it takes the ith electron $(t_{0,i})$ to reach the anode is

$$g = \frac{e}{m}\left\{E_{\mathrm{st}}\frac{1}{2}t_{0,i}^2 - \frac{E_{\mathrm{L}}}{\omega^2}\left[\cos(\omega t_{0,i}+\psi_i) - \cos(\psi_i) + \omega t_{0,i}\sin(\psi_i)\right]\right\}. \tag{5}$$

Evidently, this time can be made *independent* of the laser's amplitude provided two conditions are satisfied

$$\begin{aligned}\omega\, t_{0,i} &= 2\pi n_0\\ \psi_i &= 0\end{aligned} \tag{6}$$

where n_0 is an integer that, as we demonstrate next, represents the number of laser time periods it takes the particle to traverse the A-K gap. Explicitly, substituting these values [Eq. (6)] into Eq. (5), we obtain the "resonant particle" transit time

$$t_0 = \frac{g}{c}\sqrt{2\frac{mc^2}{eV_{\mathrm{st}}}}. \tag{7}$$

This is to say that the transit time (t_0) is an integer number (n_0) of laser time periods $(T_0 = \lambda_0/c)$; hence, in addition to the zero-phase condition ($\psi = 0$), we have

$$t_0 = \frac{g}{c}\sqrt{2\frac{mc^2}{eV_{\mathrm{st}}}} = n_0T_0. \tag{8}$$

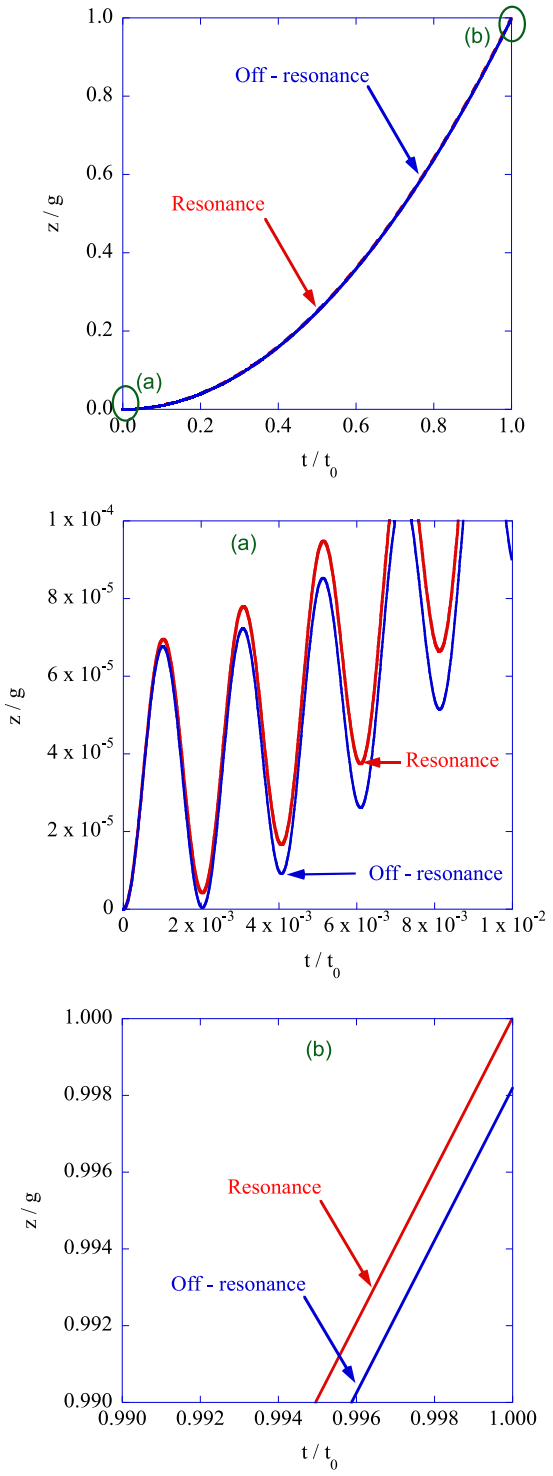

Fig. 2. Resonant (red) and off-resonance (blue) trajectories. Top frame illustrates the relevant trajectories along the entire gap — the two are indistinguishable. Central and lower frames zoom in at the input and output correspondingly. Close to the cathode, the laser field plays a dominant role and it is negligible close to the anode. The width is designed such that secondary emission electrons will play no role — see text. The parameters of the simulation: $\lambda_0 = 10.64\,[\mu\mathrm{m}]$, $E_L = 0.314\,[\mathrm{GV/m}]$, $V_{st} = 100\,[\mathrm{V}]$, $n_0 = 489$ and $g = 4.837\lambda_0$. (For interpretation of the references to color in this figure legend, the reader is referred to the web version of this article.)

These two conditions are the pillars of our paradigm and it is important to reiterate that the residue of $\mathrm{mod}\left(\frac{g}{cT_0}\sqrt{2\frac{mc^2}{eV_{st}}},1\right)=0$ as well as the fact that the energy of the emerging resonant particle is eV_{st}.

Note that in the framework of this scheme we assume a homogeneous oscillating electric field across the A-K gap. Hence, the absence of inhomogeneous field components implies the lack of nonlinear forces that can give rise to any significant ponderomotive forces acting on the electrons. More on this topic will be discussed subsequently.

3. Off-resonance conditions

Our next step is to assess the off-resonance conditions, which will indicate the amount of bunch spreading that will occur due to electrons being emitted over a finite phase of the laser field. Consider a particle whose relative phase is $\psi_i = 0 + \delta\psi_i$ and it is a small deviation from that of the resonant particle $\left(|\delta\psi_i| \ll \pi\right)$. This phase deviation causes a change in the time, $\delta t_i = t_{0,i} - t_0$, it takes this particle to traverse the A-K gap. Thus according to Eq. (5)

$$\left(1+\frac{E_{st}}{E_L}\right)(\omega\delta\tau_i)^2 + 2\frac{E_{st}}{E_L}\omega t_0(\omega\delta t_i) - 2\omega t_0\delta\psi_i = 0 \Rightarrow$$
$$\delta t_i = \frac{E_{st}}{E_{st}+E_L}t_0\left[-1+\sqrt{1+2\frac{E_L(E_{st}+E_L)}{E_{st}^2}\frac{\delta\psi_i}{\omega t_0}}\right]. \tag{9}$$

Clearly, a *stable trajectory* occurs as long as the argument of the square root is positive

$$\delta\psi_i > -\pi\frac{n_0E_{st}^2}{E_L(E_{st}+E_L)}. \tag{10}$$

In addition, we impose that the time deviation is small on the scale of one laser period $|\delta t_i| \ll T_0$; hence

$$\delta\psi_i \ll \pi\frac{n_0E_{st}^2}{E_L(E_{st}+E_L)}\left[\left(1+\frac{n_0E_{st}}{E_{st}+E_L}\right)^2-1\right]. \tag{11}$$

These last two conditions constrain the upper and lower bounds of $\delta\psi_i$ and, hence, the spread of the electrons in terms of the laser and static fields as well as the number of laser periods n_0. Note, for given values of E_L and E_{st}, that the range for acceptable values of $\delta\psi_i$ becomes less constrained for larger values of n_0. Hence, there is a benefit to operating at relatively large A-K spacing.

The phase variation among the off-resonance particles causes *velocity variations* among the emerging electrons. For determining this variation, we keep in mind that, according to Eq. (4), the velocity of the resonant particle as it reaches the anode is $v_0 = \dot{z}(t_0) = eE_{st}t_0/m$. Consequently, the velocity variation $\delta v_i = \dot{z}_i(t_{0,i}) - v_0$ is given by

$$\delta v_i = \frac{e}{m}(E_{st}+E_L)\delta t_i = v_0\left[-1+\sqrt{1+\frac{E_L(E_{st}+E_L)}{n_0E_{st}^2}\frac{\delta\psi_i}{\pi}}\right] \tag{12}$$

where we used the expression for δt_i developed in Eq. (9).

Fig. 2 gives an example of the resonant and off-resonance trajectories. We see for the set of parameters chosen that there is only a 0.2% difference in the longitudinal position between the resonant and off-resonance electrons when they arrive at the anode. Hence, the bunch spreading is negligible.

Before proceeding, it is important to quantify the constraint imposed by the condition that limits the validity of the result in Eq. (5), namely, that the field-emitted electrons do not impinge back on the cathode and generate secondary electrons. As shown in Fig. 2, we observe that if $\psi_i \neq 0$ (off-crest), the electrons after one period may impinge on the cathode and thus generate secondary electrons. While this is not destructive to our paradigm, it may alter the *energy spread* of the emerging electrons (at the anode); therefore reducing its appeal. For this reason we specify the conditions necessary to preclude this effect. According to Fig. 2 and Eq. (4), this effect occurs if an electron encounters the cathode surface after one period of the wave and implies the following two conditions

$$\dot{z}_i\left(t=t_{\rm bd}\right)=0\Rightarrow E_{\rm st}\omega t_{\rm bd}-E_{\rm L}\left[-\sin\left(\omega t_{\rm bd}+\psi_{\rm bd}\right)+\sin\left(\psi_{\rm bd}\right)\right]=0$$
$$z_i\left(t=t_{\rm bd}\right)\geq 0\Rightarrow E_{\rm st}\frac{1}{2}\omega^2 t_{\rm bd}^2-E_{\rm L}\left[\cos\left(\omega t_{\rm bd}+\psi_{\rm bd}\right)-\cos\left(\psi_{\rm bd}\right)+\omega t_{\rm bd}\sin\left(\psi_{\rm bd}\right)\right]\geq 0 \quad (13)$$

where the subscript "bd" refers to the backward-traveling electron. For most practical conditions we may assume that $E_{\rm st}\ll E_{\rm L}$ and, as such, the solution of the first condition is $\omega t_{\rm bd}\simeq 2\pi\left(1-E_{\rm st}/E_{\rm L}\right)$; therefore, the second condition indicates that we must have

$$\psi_{\rm bd}\leq\pi\frac{E_{\rm st}}{E_{\rm L}}. \quad (14)$$

As we will show later, $E_{\rm L}$ needs to be greater than $E_{\rm st}$, for example, $E_{\rm st}/E_{\rm L}\sim 0.1$. This means $\psi_{\rm bd}$ can be quite large, e.g., $\sim 0.1\pi$; hence, our paradigm can operate over a relatively wide range of the laser field phase, i.e., it is not restricted to only the very peak of the field.

4. Static space-charge effect

So far we have considered the dynamic of the electrons subject to the assumption that the electron is extracted by the combination of the two electric fields and ignoring the field generated by the electrons themselves. Next we focus our attention on the global space-charge effect on field emission and, more specifically, on the screening of the cathode by the space-charge distributed in the A-K gap. As the electron microbunches are propagating in the A-K gap, they form a charge distribution that tends to shield the cathode, thereby reducing the net field experienced by the electrons. To account for this charge shielding effect, we consider first the static effect assuming that all the electrons are uniformly distributed along the gap, and solve Poisson's equation to yield the potential in the gap

$$\Phi(z)=\frac{z}{g}\left(V_{\rm st}-\frac{eN_{\rm el}^{(AK)}}{\varepsilon_0 Ag}\frac{g^2}{2}\right)+\frac{eN_{\rm el}^{(AK)}}{\varepsilon_0 Ag}\frac{z^2}{2}. \quad (15)$$

$N_{\rm el}^{(AK)}$ is the average number of electrons traversing the A-K gap, A is the area of the cathode, and ε_0 is the vacuum permittivity. The second term in the brackets represents the field-reduction due to charge shielding. Including the static charge shielding field in the equation of motion for the resonant particle $\left(\psi_r=0\right)$ [Eq. (3)], its solution reads

$$z_r(t)=\frac{(e/m)\,E_{\rm eff}}{\omega_{\rm p}^2}\left[\cosh\left(\omega_{\rm p}t\right)-1\right]+\frac{(e/m)\,E_{\rm L}}{\omega^2+\omega_{\rm p}^2}\left[\cosh\left(\omega_{\rm p}t\right)-\cos\left(\omega t\right)\right] \quad (16)$$

wherein the plasma frequency is defined by $\omega_{\rm p}^2=e^2N_{\rm el}^{(A-K)}/m\varepsilon_0 Ag$ and the effective static electric field $E_{\rm eff}=\left(V_{\rm st}/g\right)-\left(eN_{\rm el}^{(AK)}/2\varepsilon_0 A\right)\equiv E_{\rm st}-E_{\rm SC}$. Thus, ensuring the motion is independent of E_L entails that $\cosh\left(\omega_{\rm p}t_0\right)-\cos\left(\omega t_0\right)\simeq 0$; therefore, in addition to the condition $\omega t_0=2\pi n_0$ we must impose $\omega_p^2t_0^2\ll 1$. Satisfying these requirements yields a new expression for g that includes charge shielding effects, $g=eE_{\rm eff}t_0^2/2m$, or explicitly

$$\frac{g}{\lambda_0}=-\overline{V}_{\rm sc}+\sqrt{\overline{V}_{\rm sc}^2+\overline{V}_{\rm st}} \quad (17)$$

wherein $\overline{V}_{\rm st}=n_0^2\left(eV_{\rm st}/2mc^2\right)$ and $\overline{V}_{\rm sc}=n_0^2\left(e^2N_{\rm el}^{(AK)}\lambda_0/8\varepsilon_0 Amc^2\right)$. Further, keeping in mind that the number of electrons in the A-K gap is $N_{\rm el}^{(AK)}=n_0\times$ *number of electrons in one bunch* and ignoring transients associated with the head of the train of micro-bunches, the charge per unit surface area in the A-K gap is given by the following integral equation

$$\frac{N_{\rm el}^{(AK)}}{A}=n_0\frac{10^4}{e}\int_{T_0/2}^{3T_0/2}dt\times J_{FN}\left\{\frac{\beta}{100}\left[\frac{V_{\rm st}}{g}-\frac{e}{2\varepsilon_0}\frac{N_{\rm el}^{(AK)}}{A}+E_{\rm L}\cos\left(\omega t\right)\right]\right\}. \quad (18)$$

Table 1
Typical parameters and results of the dc SC simulation.

λ_0 [μm]	10.64		
Δ_y [mm]	1		
$\Delta_{\rm strip}$ $[\lambda_0]$	0.5		
β	100		
g $[\lambda_0]$	5.0		
n_0	500		
$N_{\rm el}^{(1)}$	1000	100	10
$V_{\rm st}$ $[V]$	147.4	106.7	102.6
$E_{\rm st}$ [MV/m]	2.771	2.006	1.929
$E_{\rm SC}$ [MV/m]	0.849	0.085	0.008
$E_{\rm eff}$ [MV/m]	1.921	1.921	1.921
E_L [GV/m]	0.033	0.029	0.026
σ	0.035	0.033	0.032
$J_{\rm max}$ [A/cm^2]	973.16	102	10.65

Table 1 summarizes the parameters values for a representative numerical integration of Eq. (18) with the last seven lines in the table yielding the final results. The elliptical function was approximated by $f(x)=1-x^{1.69}$. The number of electrons in one microbunch is varied over a wide range, i.e., $N_{\rm el}^{(1)}=10,100,1000$, while at the same time adjusting the values of the other parameters, e.g., $E_{\rm st}$, in order to maintain a geometry of $g=5\lambda_0$. The resulting current density pulses are within an excellent approximation (0.1%) Gaussian with a normalized standard deviation of $\sigma\sim 0.03\,(11^o)$, namely, $\exp\left[-\frac{1}{2}\left(\frac{ct/\lambda_0}{\sigma}\right)^2\right]$, and with peak values of $J_{\rm max}\left[{\rm A/cm^2}\right]\sim 10.6,\,102\,,973$, respectively. This 11° phase range demonstrates the relatively wide acceptance range that is possible [see Eq. (14)].

Note that the net static field $\left(E_{\rm eff}=E_{\rm st}-E_{\rm SC}\right)$ is constant despite the fact the number of electrons in the microbunch changes by a two orders of magnitude. Therefore, we conclude that this exponential growth of the current density is due to the laser field $\left(E_{\rm L}\right)$ and the field enhancement factor(β). However, interestingly, the magnitude of the laser field does not change appreciably as $N_{\rm el}^{(1)}$ increases and the ratio $E_{\rm st}/E_{\rm L}$ remains roughly constant, i.e., ~ 0.1.

The minute standard deviation (σ) of the current density for a given bunch that is achievable following the proposed approach is a numerical demonstration of the bandwidth control expressed in Eqs. (10)–(11), thereby revealing the potential of the proposed paradigm.

It should be pointed out that the Child–Langmuir (CL) limiting current density, for $V_{\rm st}\sim 100$ V and $g\sim 5\lambda_0$, namely $J_{\rm CL}\simeq 52$ A/cm^2, is a factor of 17 higher than the average current density $J_{\rm max}\times\sigma\sim 3$ A/cm^2 — considering the middle column in Table 1. However, it is half the peak current density, which is consistent with results reported in the literature whereby perveance more than twice CL was measured [27] for the case of short pulses.

5. Energy spread

The control we have with the static and laser field components on the current density emitted at the *cathode* affects also the energy spread of the electrons reaching the *anode*. For an estimate, let us examine the resonant particle trajectory $z_r\left(t_0\right)=g$ and the question is what is the energy-spread resulting from the finite bunch duration at the location of its generation plane ($z=0$), namely, at the cathode. With the Gaussian distribution mentioned above, $G(t,\sigma)=\frac{c}{\lambda_0\sigma}\frac{1}{\sqrt{2\pi}}\exp\left[-\frac{1}{2}\left(\frac{ct}{\lambda_0\sigma}\right)^2\right]$, the average velocity of an electron when reaching the anode is

$$\langle\dot{z}\rangle=\int_{-\infty}^{\infty}dtG(t,\sigma)\,\dot{z}\left(t_0+t\right)\simeq\dot{z}_r\left(t_0\right)+\frac{1}{2}\left(\frac{\sigma\lambda_0}{c}\right)^2\dddot{z}_r\left(t_0\right) \quad (19)$$

in a similar way, the standard deviation is

$$(\Delta\dot{z})^2=\int_{-\infty}^{\infty}dtG(t,\sigma)\left[\dot{z}\left(t_0+t\right)-\langle\dot{z}\rangle\right]^2\simeq\left(\frac{\sigma\lambda_0}{c}\right)^2\ddot{z}_r^2\left(t_0\right). \quad (20)$$

Consequently, the relative energy spread at the anode is proportional to the current density spread at the cathode

$$\frac{(\Delta\dot{z})^2}{\langle\dot{z}\rangle^2} \simeq \left(\frac{\sigma\lambda_0}{c}\right)^2 \frac{\ddot{z}_r^2(t_0)}{\dot{z}_r^2(t_0)} \simeq \frac{E_{\mathrm{L}}^2}{n_0^2 E_{\mathrm{st}}^2} \sim 10^{-4} \tag{21}$$

which, for the parameters in Table 1, is of the same order of magnitude as that of RF photo-injectors.

It is important to emphasize that the Gaussian distribution of the emitted electrons is not accidental nor a result of a specific set of parameters. If we return to the revised Fowler-Nordheim formula, Eq. (1), and assume the peak current occurs at $t = 0$, then the peak field (F) intensity occurs at the same time implying that

$$\frac{F(t)}{F_{\mathrm{cr}}[F(t)]} \simeq C_0 - C_2 t^2 \tag{22}$$

up to a second-order Taylor expansion, where C_0 and C_2 represent the appropriate coefficients. Substituting in Eq. (1), when sufficiently apart from the peak value of the current density, the exponential term is dominant; therefore

$$J_{\mathrm{FN}} \propto \exp\left[-\left(C_2/C_0^2\right)t^2\right]. \tag{23}$$

6. Dynamic space-charge effect

To recapitulate, our first step was to demonstrate the concept by neglecting space-charge effects. The second step was to account for the static charge shielding effect assuming that the charge associated with the emitted electrons is *uniformly* distributed within the A-K gap. It was shown that this affects the emission, but this effect does not change the energy of the microbunches since each electron is slightly decelerated during the first half of the gap and it is slightly accelerated by the same amount during the second half. On the other hand, although the repulsion of the electrons from each other has negligible effect on the emission process, it can cause the microbunches to lengthen and this may become detrimental for the electrons emerging from the anode.

We have simulated this dynamic space-charge effect by adding the space charge term to Eq. (3)

$$\begin{aligned}\frac{d^2 z_i}{dt^2} &= \frac{e}{m}\left[E_{\mathrm{st}} + E_{\mathrm{L}}\cos(\omega t + \psi_i)\right] \\ &\quad - \frac{e^2 N_{\mathrm{el}}^{(AK)}}{m\varepsilon_0 A g}\frac{1}{2}\left[1 - 2\left\langle h\left(z_i - z_{i'}\right)\right\rangle_{i'}\right]\end{aligned} \tag{24}$$

and simulation results indicate negligible effect for the relevant parameters — consistent with the results reported in [9]. For a quantitative measure of the de-bunching process, we follow the same approach used in the previous section for the energy spread, but this time applied to the space charge effect, namely

$$\begin{aligned}\langle z\rangle &= \int_{-\infty}^{\infty} dt G(t,\sigma)\, z_r(t_0 + t) \\ &\simeq z_r(t_0) + \frac{1}{2}\ddot{z}_r(t_0)\int_{-\infty}^{\infty} dt G(t,\sigma)\, t^2 \\ &\simeq z_r(t_0) + \frac{1}{2}\left(\frac{\sigma\lambda_0}{c}\right)^2 \ddot{z}_r(t_0) \\ \left\langle z^2\right\rangle &= \int_{-\infty}^{\infty} dt G(t,\sigma)\, z_r^2(t_0 + t) \simeq z_r^2(t_0) \\ &\quad + \left(\frac{\sigma\lambda_0}{c}\right)^2 \left[z_r(t_0)\ddot{z}_r(t_0) + \dot{z}_r^2(t_0)\right].\end{aligned} \tag{25}$$

The longitudinal spread is $\Delta^2\left(t_0, \omega_{\mathrm{p}}^2\right) \equiv \left\langle z^2\right\rangle - \langle z\rangle^2 \simeq \left(\frac{\sigma\lambda_0}{c}\right)^2 \dot{z}_r^2(t_0)$ and, consequently, the relative change in the spread due to the space charge effect is

$$\left|\frac{\Delta^2\left(t_0, \omega_{\mathrm{p}}^2\right) - \Delta^2\left(t_0, \omega_{\mathrm{p}}^2 \simeq 0\right)}{\Delta^2\left(t_0, \omega_{\mathrm{p}}^2 \simeq 0\right)}\right| \simeq 2\frac{E_{\mathrm{SC}}}{E_{\mathrm{st}}}. \tag{26}$$

According to the simulation results presented in Table 1, the de-bunching is negligible for the case of 10 electrons in the microbunch (0.8%); it is acceptable for the case of 100 electrons (8%); and it becomes very significant (> 60%) with 1000 electrons in the microbunch.

An interesting observation is revealed by this dynamic space-charge simulation [Eq. (24)]. Since the velocity of the electrons varies in the A-K gap, the temporal and spatial structure changes within the gap. While the *time* difference between two peaks is always equal to the laser period (T_0), the *spacing* between two peaks varies according to the velocity of the microbunches. Qualitatively, the spacing between two adjacent microbunches (Δ_{mb}) located in the vicinity of a point z may be described by

$$\Delta_{\mathrm{mb}}(z) \simeq \lambda_0\sqrt{\frac{1}{2}\frac{eE_{\mathrm{st}}z}{mc^2}}. \tag{27}$$

Clearly, the spacing between any two adjacent bunches is small near the cathode and it reaches maximum at the anode. This is in contrast to a relativistic beam where it can be shown that at the anode, $\Delta_{\mathrm{mb}} \simeq \lambda_0$. Despite this spatial "distortion" at very low velocities, our analysis indicates the microbunch temporal distribution at the anode is essentially Gaussian (error of less than 0.1%).

7. Emittance

Our goal in the framework of the current study is to demonstrate conceptually the paradigm with minimum mathematical complexity. In this process we ignored 3D electrostatic effects associated with the anode aperture through which the microbunches exit the injector. It is tacitly assumed that these effects can be reduced by curving the cathode as is done in relativistic klystrons [28] or employing electrostatic focusing, such as multiple electrodes, as done in Spindt field array systems [29]. In a similar manner, these same self-focusing designs can be used to control defocusing effects at the anode, which in our scheme we envision to be a single, microscopic aperture.

While the impact of transverse geometry on beam dynamics can be minimized, *a-priori* it is not obvious that a similar treatment will succeed for the magnetic field associated with the wave and its transverse variation (x). In this section, we consider not only the electric field $E_z = -E_{\mathrm{L}}\cos\left[\omega(t - x/c)\right]$, but also the magnetic field component $H_y = \left(E_{\mathrm{L}}/\eta_0\right)\cos\left[\omega(t - x/c)\right]$, as well as transverse variations so that the dynamics are determined by the following equations of motion

$$\begin{aligned}\frac{d^2\bar{z}_i}{d\tau^2} &= \bar{E}_{\mathrm{st}} + \bar{E}_{\mathrm{L}}\left(1 - \frac{d\bar{x}_i}{d\tau}\right)\cos\chi_i - \frac{1}{2}\bar{\omega}_{\mathrm{p}}^2\left[1 - 2\left\langle h\left(\bar{z}_i - \bar{z}_{i'}\right)\right\rangle_{i'}\right] \\ \frac{d^2\bar{x}_i}{d\tau^2} &= \bar{E}_{\mathrm{L}}\frac{d\bar{z}_i}{d\tau}\cos\chi_i\end{aligned} \tag{28}$$

where the coordinates are normalized with the wavelength, the time $\tau = ct/\lambda_0$, and the phase is defined as $\chi_i = 2\pi\left(\tau - \bar{x}_i\right)$. Assuming the average location of the ensemble of particles and their normalized velocity at the *cathode* vanish, i.e., $\left\langle\bar{x}_i(0)\right\rangle = 0$ and $\left\langle\dot{\bar{x}}_i(0)\right\rangle = 0$, the emittance at the output based on Lapostolle's definition, is

$$\begin{aligned}\frac{\varepsilon_x^2(\tau_0)}{16\lambda_0^2} &\simeq \left\langle\left[\bar{x}_i(\tau_0) - \left\langle\bar{x}_{i'}(\tau_0)\right\rangle_{i'}\right]^2\right\rangle_i \left\langle\left[\dot{\bar{x}}_i(\tau_0) - \left\langle\dot{\bar{x}}_{i'}(\tau_0)\right\rangle_{i'}\right]^2\right\rangle_i \\ &\quad - \left\langle\left[\bar{x}_i(\tau_0) - \left\langle\bar{x}_{i'}(\tau_0)\right\rangle_{i'}\right]\left[\dot{\bar{x}}_i(\tau_0) - \left\langle\dot{\bar{x}}_{i'}(\tau_0)\right\rangle_{i'}\right]\right\rangle_i^2.\end{aligned} \tag{29}$$

Analytic examination of this expression indicates that it is independent of the bunch spread σ^2; which is to say that the emittance is given by

$$\varepsilon_x^2(\tau_0) \simeq \varepsilon_x^2(0) + \mathrm{O}\left(\sigma^4\right). \tag{30}$$

It warrants to also point out that the emittance is independent of the amplitude of the laser field — see Appendix. These are two additional results that are pivotal features of our paradigm.

Two interesting features as revealed in Appendix warrant special attention: (i) subject to the current design, the average transverse velocity is zero at the cathode and anode, i.e., $\left\langle\dot{\bar{x}}_i(\tau_0)\right\rangle = \left\langle\dot{\bar{x}}_i(0)\right\rangle = 0$.

In addition, the average transverse velocity spread is also constant $\left\langle \dot{\bar{x}}_i^{\,2}(\tau_0)\right\rangle = \left\langle \dot{\bar{x}}_i^{\,2}(0)\right\rangle$. (ii) Notwithstanding these zero average velocities, there is still a very small net transverse movement due to the magnetic field. Since the wave propagates in the positive direction of the x-axis, the electron ensemble is slightly pushed forward $\left\langle \bar{x}_i(\tau_0)\right\rangle = \tau_0 \bar{E}_{\mathrm{L}}^2 (4\pi)^{-2}$; this is a minuscule $\left\langle x_i(t_0)\right\rangle = 10^{-11}$m effect, but evidently it is not identically zero.

It warrants to point out that Eq. (28) also allows us to establish transient effects. From the onset, we assumed a steady-state operation regime, therefore the question is on what time scales this regime is reached. Solution of Eq. (28) indicates that, for the parameters employed in the present analysis, equilibrium is reached in less than 50 temporal periods of the laser field. The first dozen microbunches are somewhat broader and each one contains more electrons than the rest of the microbunches. This can be readily understood since for the first few microbunches, the shielding due to the presence of the charge in the A-K gap is negligible and the maximum electric field experienced by the cathode is significantly larger. As a result, the current density is higher than during steady state operation. Moreover, the microbunch duration is longer since the threshold for emission is exceeded for an extended period. We should indicate that these values assume a sharp rise time (step function) of the laser field and no attempt has been made to taper this rise time. Doing so may reduce significantly the transient time it takes the system to reach steady state.

8. Discussion

An important ramification of our paradigm is we are operating in a field-emission dominated mode rather than a photoemission-dominated one as demonstrated by Hommelhoff, et al., [9]. As a consequence, the applied laser field simply adds to the static field, thereby enhancing the amount of field emission current via the FN equation [Eq. (1)], but without affecting the energy of the electrons at the anode nor their energy spread. To accomplish this requires satisfying a specific relationship between the values of g, V_{st} and n_0 via Eq. (8). Moreover, in order to help counter charge shielding affects, one would like to operate at high values for E_{L}; however, the ratio of $E_{\mathrm{st}}/E_{\mathrm{L}}$ should be kept as large as possible while still satisfying the constraint that $E_{\mathrm{st}} \ll E_L$. This helps ensure an appreciable fraction of the laser field phase is able to participate in the field emission process while minimizing the amount of backward traveling electrons [see Eq. (14)]. Hence, E_{st} should also be as large as possible while still avoiding significant self-field emission. Fortunately, a high laser field also suppresses the field emission when E_{L} is in the negative direction; thus, this should allow operating at relatively high values of E_{st} without causing self-field emission.

The wavelength of the laser can have a significant impact on the output of the electron source. A longer wavelength permits a higher amount of charge to be emitted per laser cycle while still being constrained by the same space-charge limitations. This is because emission of electrons, whose density is independent of the laser wavelength, occurs over a longer time duration. A longer wavelength also means the illuminated area of the cathode will be correspondingly larger as well as the other physical dimensions of the electron source, such as the gap size. The larger dimensions will ease construction of the source. Hence, in principle, a CO_2 laser ($\lambda_0 = 10.6$ μm) can generate orders of magnitude higher charge than a Nd:YAG laser ($\lambda_0 = 1.06$ μm). However, the phase stability of the laser is important; otherwise, there will be temporal jitter of the emitted microbunches. For this reason, a mode-locked laser should be used.

In the framework of the present analysis, the emission process was represented by the field emission enhancement factor (β) incorporated in the Fowler–Nordheim (corrected) formula. This factor accounts for natural microscopic protrusions or man-made geometric features. For example, emission can be from a metallic edge [30] where the current density can reach values 10^9 A/cm^2, limited by the evaporation of the material. However, if the metallic tips are in close proximity to each other, then it is possible for the tips to short-circuit the electric fields of adjacent tips, thereby, effectively making the array of tips act like a flat surface. We have demonstrated [31] for a metallic grating that there is an optimum distance of separation between the edges, which still yields enhancement of the field while minimizing short-circuiting effects. Periodic bundles of CNTs could be fabricated using this same design strategy.

Since we mentioned evaporation, we should consider the stability of the emission from the CNTs. When multiple tips or sites are emitting, there is initially unequal emission from the tips. As such, as one site erodes, the current is diverted to an adjacent site with a corresponding increase in emission. However, Spindt, et al., [32] demonstrated that by conditioning an array of metallic tips, the emission can be stabilized. A similar conditioning process has been applied to an array of vertically-oriented CNTs where, after conditioning, emission followed the expected FN behavior resulting in < 30% variation in the emission current over the array of CNT emitters [33]. As shown in the photomicrographs of the individual CNTs in [33], each CNT had the same height within a small fraction of 1 μm.

Assuming that the emitting cathode has been conditioned, the next source of jitter in the bunch is the DC power supply, since by setting the A-K gap such that the transit time of the electrons is an integer number of laser periods, the emission of electrons will be primarily a function of the static field. Hence, the energy spread of the electrons will be determined by the stability of the static field. Ultra-stable, high-voltage DC power supplies are readily available, thereby ensuring very low energy spread. Furthermore, the A-K gap can be precisely set utilizing piezoelectric-controlled micrometers that are available with 5 nm resolution [34]. The absolute gap distance can be measured with a non-contact capacitance probe that has < 0.1 μm resolution [35]. As mentioned, the anode is assumed to be a single microscopic aperture rather than a grid to permit injecting the electrons as a single beam into the DLA accelerating channel. This has the advantage of facilitating maintaining a precise A-K spacing while avoiding problems with needing a flat anode grid. Located between the injector and DLA structure, could be an acceleration cavity powered by a high voltage pulsed source (e.g., > 100 kV to ~1 MV) to increase the energy of the fs-microbunches entering the DLA. E-beam focusing optics can also be used to focus the beam into the DLA.

Although 100 electrons per microbunch seems small, it should be kept in mind these microbunches are being generated every optical period of the laser beam. For a laser beam operating at 10.6 μm, this means the repetition rate of the pulse train being emitted from the injector is 2.8×10^{13} Hz! With 100 electrons per microbunch, this corresponds to an average current of 0.45 mA. If the laser pulse duration is, say, 100 ns, then there will be 2.8×10^8 electrons (45 pC) per laser pulse. Hence, the total number of electrons emitted from the injector can be useful for many applications.

We have also demonstrated in the framework of the proposed paradigm that the transverse emittance is preserved and a relative energy spread of less than 0.01% may be anticipated.

Acknowledgments

This work was supported by the Israel Science Foundation (1135/14) and by internal research and development funds provided by STI Optronics, Inc.

Appendix

Our goal in this Appendix is to develop an approximate solution of Eq. (28) in order to assess the transverse emittance. Keeping in mind that the motion is not relativistic and assuming, for the purpose of estimating the transverse emittance, that the longitudinal structure of the beam is sufficiently symmetric such that we can employ

$$\frac{1}{2}\bar{\omega}_{\mathrm{p}}^2\left[1-2\left\langle h\left(\bar{z}_i-\bar{z}_{i'}\right)\right\rangle_{i'}\right] \rightarrow \frac{1}{2}\bar{\omega}_{\mathrm{p}}^2\left(1-2\frac{\lambda_0}{g}\bar{z}_i\right) \tag{31}$$

then Eq. (28) simplifies to

$$\begin{aligned}\frac{d^2\bar{z}_i}{d\tau^2} &= \bar{E}_{\rm st} + \bar{E}_{\rm L}\left(1-\frac{d\bar{x}_i}{d\tau}\right)\cos\chi_i - \frac{1}{2}\bar{\omega}_{\rm p}^2\left(1-2\frac{\lambda_0}{g}\bar{z}_i\right)\\ \frac{d^2\bar{x}_i}{d\tau^2} &= \bar{E}_{\rm L}\frac{d\bar{z}_i}{d\tau}\cos\chi_i.\end{aligned} \tag{32}$$

Subject to the previous assumptions and to the resulting estimates, the longitudinal dynamics [Eq. (16)] may be approximated by

$$\begin{aligned}\bar{z} &= \left(\bar{E}_{\rm st}-\frac{1}{2}\bar{\omega}_{\rm p}^2\right)\frac{1}{2}\tau^2 + \frac{1}{(2\pi)^2}\bar{E}_{\rm L}\left[1+\frac{1}{2}\bar{\omega}_{\rm p}^2\tau^2-\cos(2\pi\tau)\right]\\ \dot{\bar{z}} &= \left(\bar{E}_{\rm st}-\frac{1}{2}\bar{\omega}_{\rm p}^2\right)\tau + \frac{1}{(2\pi)^2}\bar{E}_{\rm L}\left[\bar{\omega}_{\rm p}^2\tau+2\pi\sin(2\pi\tau)\right]\end{aligned} \tag{33}$$

whereas the transverse trajectory is given by

$$\begin{aligned}\bar{x}(\tau) &= \bar{x}(0)+\tau\dot{\bar{x}}(0)\\ &+\bar{E}_{\rm L}\left\{\begin{array}{l}\left(\bar{E}_{\rm st}-\frac{1}{2}\bar{\omega}_{\rm p}^2+\frac{\bar{E}_{\rm L}}{(2\pi)^2}\right)\frac{2\bar{\omega}_{\rm p}^2}{(2\pi)^3}\left[\sin(2\pi\tau)-\pi\tau\cos(2\pi\tau)\right]\\ +\frac{\tau}{4}\frac{\bar{E}_{\rm L}}{(2\pi)^2}\left[1-\operatorname{sinc}(4\pi\tau)\right]-\left(\bar{E}_{\rm st}-\frac{1}{2}\bar{\omega}_{\rm p}^2+\frac{\bar{E}_{\rm L}}{(2\pi)^2}\right)\frac{\bar{\omega}_{\rm p}^2\tau}{(2\pi)^2}\end{array}\right\}\\ \dot{\bar{x}}(\tau) &= \dot{\bar{x}}(0)\\ &+\bar{E}_{\rm L}\left\{\begin{array}{l}\left(\bar{E}_{\rm st}-\frac{1}{2}\bar{\omega}_{\rm p}^2+\frac{\bar{E}_{\rm L}}{(2\pi)^2}\right)\frac{\bar{\omega}_{\rm p}^2}{(2\pi)^2}\left[\cos(2\pi\tau)+2\pi\tau\sin(2\pi\tau)\right]\\ +\frac{1}{2}\frac{\bar{E}_{\rm L}}{(2\pi)^2}\sin^2(2\pi\tau)-\left(\bar{E}_{\rm st}-\frac{1}{2}\bar{\omega}_{\rm p}^2+\frac{\bar{E}_{\rm L}}{(2\pi)^2}\right)\frac{\bar{\omega}_{\rm p}^2}{(2\pi)^2}\end{array}\right\}.\end{aligned} \tag{34}$$

When the particle approaches the anode $\tau=\tau_0$, its transverse location is $\bar{x}_i(\tau_0)=\bar{x}_i(0)+\tau_0\dot{\bar{x}}_i(0)+\tau_0\bar{E}_{\rm L}^2(4\pi)^{-2}$; thus, assuming the average location at the anode is at the center, $\langle\bar{x}_i(0)\rangle=0$, and the corresponding average velocity is zero, $\langle\dot{\bar{x}}_i(0)\rangle=0$, then

$$\begin{aligned}\langle\bar{x}_i(\tau_0)\rangle &= \tau_0\bar{E}_{\rm L}^2(4\pi)^{-2}\\ \langle\bar{x}_i^2(\tau_0)\rangle &= \langle\bar{x}_i^2(0)\rangle+\tau_0^2\langle\dot{\bar{x}}_i{}^2(0)\rangle+\left[\tau_0\bar{E}_{\rm L}^2(4\pi)^{-2}\right]^2\\ \langle\dot{\bar{x}}_i(\tau_0)\rangle &= 0\\ \langle\dot{\bar{x}}_i(\tau_0)\bar{x}_i(\tau_0)\rangle &= \tau_0\langle\dot{\bar{x}}_i{}^2(0)\rangle\\ \langle\dot{\bar{x}}_i{}^2(\tau_0)\rangle &= \langle\dot{\bar{x}}_i{}^2(0)\rangle.\end{aligned} \tag{35}$$

Substituting these approximate solutions in the expression for the transverse emittance [Eq. (29)], we obtain the result in Eq. (30), which indicates that the transverse emittance is conserved in spite of the presence of the laser field.

References

[1] R. Joel England, Robert J. Noble, Karl Bane, David H. Dowell, Cho-Kuen Ng, James E. Spencer, Sami Tantawi, Ziran Wu, Robert L. Byer, Edgar Peralta, Ken Soong, Chia-Ming Chang, Behnam Montazeri, Stephen J. Wolf, Benjamin Cowan, Jay Dawson, Wei Gai, Peter Hommelho_, Yen-Chieh Huang, Chunguang Jing, Christopher McGuinness, Robert B. Palmer, Brian Naranjo, James Rosenzweig, Gil. Travish, Amit Mizrahi, Levi Schachter, Christopher Sears, Gregory R. Werner, Rodney B. Yoder, Rev. Modern Phys. 86 (2014) 1337.

[2] B.M. Cowan, Phys. Rev. ST Accel. Beams 6 (2003) 101301.

[3] L. Schachter, Phys. Rev. E 68 (2003) 036502.

[4] E.A. Peralta, K. Soong, R.J. England, E.R. Colby, Z. Wu, B. Montazeri, C. McGuinness, J. McNeur, K.J. Leedle, D. Walz, E.B. Sozer, B. Cowan, B. Schwartz, G. Travish, R.L. Byer, Nature 503 (2013) 9194.

[5] V. Karagodsky, D. Schieber, L. Schachter, Phys. Rev. Lett. 104 (2010) 024801.

[6] W.D. Kimura, L. Schachter, Phys. Rev. Lett. 114 (2015) 195501.

[7] Z. Toroker, L. Schachter, Phys. Rev. Special Topics – Accelerators and Beams 18 (2015) 071301.

[8] M. Voin, L. Schachter, Phys. Rev. Special Topics - Accelerators and Beams 18 (2015) 071302.

[9] P. Hommelhoff, Yvan Sortais, Anoush Aghajani-Talesh, Mark A. Kasevich, Phys. Rev. Lett. 96 (2006) 077401.

[10] R. Ganter, R. Bakker, C. Gough, S.C. Leemann, M. Paraliev, M. Pedrozzi, F. Le Pimpec, V. Schlott, L. Rivkin, A. Wrulich, Phys. Rev. Lett. 100 (2008) 064801.

[11] Hirofumi Yanagisawa, Christian Hafner, Patrick Don, Martin Klckner, Dominik Leuenberger, Thomas Greber, Jrg Osterwalder, Matthias Hengsberger, Phys. Rev. B 81 (2010) 115429.

[12] F.M. Charbonnier, J.P. Barbour, L.F. Garrett, W.P. Dyke, Proc. IEEE 51 (1963) 9911004.

[13] P.M. Lally, Y. Goren, E.A. Nettesheim, IEEE Trans. Electron Devices 36 (1989) 2738–2741.

[14] R.E. Neidert, M. Phillips Purobi, S.T. Smith, C.A. Spindt, IEEE Trans. Electron Devices 38 (1991) 661–665.

[15] C. Hernandez-Garcia, C.A. Brau, Nucl. Instrum. Methods Phys. Res. A 429 (1999) 257–263.

[16] C. Hernandez-Garcia, C.A. Brau, Nucl. Instrum. Methods Phys. Res. A 475 (2001) 559–563.

[17] C. Hernandez-Garcia, C.A. Brau, Nucl. Instrum. Methods Phys. Res. A 483 (2002) 273–276.

[18] R.H. Fowler, L. Nordheim, Proc. R. Soc. A 119 (1928) 173–181.

[19] J.P. Barbour, W.W. Dolan, J.K. Trolan, E.E. Martin, W.P. Dyke, Phys. Rev. 92 (1953) 45–51.

[20] L. Nordheim, Proc. R. Soc. A 121 (1928) 626–639.

[21] J.M. Houston, Phys. Rev. 88 (1952) 349.

[22] R.E. Burgess, H. Kroemer, J.M. Houston, Phys. Rev. 90 (1953) 515.

[23] F. Le Pimpec, C. Gough, V. Chouhan, S. Kato, Nucl. Instrum. Methods Phys. Res. A 660 (2011) 7–14.

[24] J.-M. Bonard, N. Weiss, H. Kind, T. Stckli, L. Farr, Klaus Kern, A. Chtelain, Adv. Mater. 13 (2001) 184–188.

[25] H. Murakami, M. Hirakawa, C. Tanaka, H. Yamakawa, Appl. Phys. Lett. 76 (2000) 1776–1778.

[26] J. Ho Rogge, J.P. Stein, M. Krger, M. Frster, J. Hammer, D. Ehberger, P. Baum, P. Hommelho_, Appl. Phys. J. 115 (2014) 094506.

[27] R.K. Parker, Richard E. Anderson, Charles V. Duncan, J. Appl. Phys. 45 (1974) 2463.

[28] D. Sprehn, R.M. Phillips, G. Caryotakis, SLAC-PUB-6677, September 1994, Presented at the 40 Anniversary IEEE International Electron Devices Meeting, San Francisco, CA, December 11-14, 1994.

[29] C.A. Spindt, J. Appl. Phys. 39 (7) (1968) 3504–3505;
A.A. Talin, K.A. Dean, J.E. Jaskie, Solid-State Electronics 45 (6) (2001) 963976;
J.A. Nation, L. Schachter, F.M. Mako, L.K. Len, W. Peter, F.M. Mako, Cha-Mei Tang, T. Srinivasan-Rao, Proc. IEEE 87 (5) (1999) 865-889.

[30] L. Schachter, Appl. Phys. Lett. 72 (4) (1998) 421–423.

[31] B. Haddad, L. Schachter, Appl. Phys. Lett. 74 (1999) 1180–1182.

[32] P.R. Schwoebel, C.A. Spindt, C.E. Holland, J.A. Panitz, J. Vac. Sci. Technol. B 19 (2) (2001) 582–585;
P.R. Schwoebel, C.A. Spindt, C.E. Holland, A. Panitz, J. Vac. Sci. Technol. B 19 (3) (2001) 980-988.

[33] V. Semet, V. Thien Binh, P. Vincent, D. Guillot, K.B.K. Teo, M. Chhowalla, G.A.J. Amaratunga, W.I. Milne, P. Legaganeux, D. Pribat, Appl. Phys. Lett. 81 (2002) 343–345.

[34] See for example, Thorlabs Model DRV120 Modular NanoMax 20 m Piezo Drive.

[35] See for example, Microsense Model 4810 with Model 2803 capacitance probe.